Effects of cascading optical processes: Part III. impacts on spectroscopic measurements of fluorescent samples

Max Wamsley, $^{\Diamond, \#}$ Pathum Wathudura, $^{\Diamond, \#}$ Samadhi Nawalage $^{\Diamond, \#}$ Shengli Zou, $^{\Delta}$ and Dongmao Zhang $^{\Diamond, *}$

[⋄] Department of Chemistry, Mississippi State University, Mississippi State, MS 39762, United States

[∆] Department of Chemistry, University of Central Florida, Orlando, FL 32816, United States.

*Dongmao Zhang; dongmao@chemistry.msstate.edu; (662)-325-6752

Equal contributions

ABSTRACT

Cascading optical processes refer to two or more sequential photon/matter interactions triggered by the same individual excitation photons. The previous two parts of this examined cascading optical processes in scattering-only solutions (Part I) and samples containing light scatterers and absorbers, but no emitters (Part II). The current work (Part III) focuses on the effects of cascading optical processes on spectroscopic measurements of fluorescent samples. Four types of samples are used in this study, including 1) Eosin Y (EOY), an absorber and emitter; 2) EOY mixed with plain polystyrene nanoparticles (PSNPs) that are pure scatterers; 3) EOY mixed with dyed PSNP that are scattering- and absorbing-, but not emitting nanoparticles; and 4) fluorescent PSNPs that are simultaneous light absorbers, scatterers, and emitters. Interference from both forward scattered and emitted photons can cause nonlinearity and spectral distortion in UV-vis extinction measurements. Sample absorption by nonfluorogenic chromophores invariably reduces fluorescence intensity, where the effect of scattering on fluorophore fluorescence is complicated by several competing factors. A revised first-principles model is developed for correlating the experimental fluorescence intensity with the sample absorbance in solutions containing both scatterers and absorbers. The optical properties of fluorescent PSNPs of three different sizes were systematically investigated using combined measurements with integratingsphere-assisted resonance synchronous spectroscopy, linearly polarized resonance synchronous spectroscopy, UV-vis, and fluorescence spectroscopy. The insights and methodology provided in this work should help improve the reliability of spectroscopic analyses of fluorescent samples, where the interplay among light absorption, scattering, and emission can be highly complicated.

INTRODUCTION

Cascading optical processes refer to two or more sequential optical events triggered by individual excitation photons. Such sequential optical events can be of the same (e.g., scattering of the scattered photons) or different mechanistic origins (e.g., emission after absorption). In Part I and II of these three companion articles, we presented the cascading optical processes in scattering-only samples (Part I) and solutions that contain both scatterers and absorbers, but not emitters (Part II).^{1, 2} While the cascading optical process in scattering-only samples is relatively simple, as it involves only multiple scatterings, its impact on spectroscopic measurements is significant. It complicates scattering extinction, intensity, and depolarization analysis even when the sample concentration is within the linear dynamic range (LDR) of the UV-vis spectrophotometer.^{1,3,4}.

The additional interplay between light absorption and scattering makes the cascading optical processes in light-absorbing, scatterer-containing samples far more complicated than that in the scatterer-only solutions.² Light absorption invariably reduces the scattering intensity due to the absorption inner-filter-effect (IFE).⁵⁻⁷ However, the impact of scattering on light absorption is complicated, depending on whether the scattered light is taken into consideration. Scattering reduces light absorption along the linear optical path from the excitation source to the UV-vis detector. However, absorption of the scattered photons can partially, totally, and even overcompensate for such reduced light absorption. Imaginably, the degree to which the scattered light is absorbed depends not only on the solution volume, sample absorption, and scattering activities, but also the cuvette geometry. In part II, we systematically examined the impact of scattering on the total light absorption, including the absorption of the scattered photons for samples with a solution volume of 3 mL in a 1-cm square cuvette. In such a case, the total light absorption of the scatterer-containing samples is approximately the same as their respective scatterer-free

counterparts, with the same absorption extinction.² The presence of scatterers in those samples changes the locations where light absorption occurs but does not significantly modify the amount of light absorption.²

The present work (Part III) focuses on the cascading optical processes in fluorescent solutions and their impacts on sample UV-vis, scattering, and fluorescence measurements. Mechanistically, the cascading optical processes in fluorescent samples can be extraordinarily complicated. Even for solutions containing only one molecular fluorophore, there are two sequential optical events: absorption and emission. Numerous additional cascading processes can occur if the fluorophore also absorbs at the emission wavelengths. In this case, the emitted photons can be reabsorbed, possibly triggering further emission, reabsorption, and so on. In scatterer-containing fluorescent samples, the complexity of the cascading optical processes grows exponentially, because scattering can perturb the optical path of excitation and emission photons inside the solutions, consequently affecting the fluorescence signal generation and/or detection.

$$I^{corr}(\lambda_x, \lambda_m) = I(\lambda_x, \lambda_m) \times 10^{0.5A_x + 0.5A_m}$$
 (1)

$$I^{corr}(\lambda_x, \lambda_m) = I(\lambda_x, \lambda_m) \times 10^{d_x A_x + d_m A_m}$$
 (2)

Existing work on the effects of cascading optical processes on fluorescence measurements have almost exclusively been on the impacts of fluorophore or sample absorption on the fluorescence intensity. Absorption causes nonlinearity between fluorescence intensity and fluorophore concentration, as well as introduces spectral distortion. Such effects have been commonly referred to as the absorption-IFE. Many mathematical models have been developed for correcting the absorption IFE on fluorescence measurements. Eq. 1 has been popularly used for correcting the absorption-IFE on fluorescence spectra acquired with a 1-cm

square cuvette. A_x and A_m are the sample absorbances, quantified using a 1-cm path length cuvette, at the excitation and emission wavelengths, respectively.⁵ This model (Eq. 1) assumes that the instrument is perfectly aligned, so that the effective excitation and emission path lengths are both 0.5 cm in the conventional 90-degree spectrofluorometric spectral acquisition.

We previously reported a generalized model for correcting the absorption-IFE on fluorescence measurements (Eq. 2),⁷ where d_x and d_m refer to the effective light absorption and emission path lengths. These pathlengths can be readily quantified using a solvent Raman technique.⁸ This model is also useful for correcting the absorption-IFE on resonance synchronous spectra acquired with a spectrofluorometer.^{12, 13} Since the excitation and detection wavelength are the same in these spectroscopic measurements, the total absorption path length is simply the sum of d_x and d_m .

The effectiveness of Eq. 2 for correcting the absorption-IFE has been demonstrated extensively with molecular fluorophores containing no significant scattering. The absorption-IFE-corrected fluorescence intensity exhibits excellent linearity with fluorophore concentration. However, current knowledge on the effects of light scattering on fluorescence intensity has been scant. We have previously compared the effects of sample absorption and scattering on fluorophore fluorescence and concluded that, in comparison to absorption, the impact of scattering on sample fluorescence intensity is negligibly small. However, this conclusion was derived with polystyrene nanoparticles (PSNPs) of 100 nm in diameter. The overall generality of this observation is unknown. Addressing this question is important since the impacts of multiple scattering on spectroscopic measurement depends strongly on particle sizes. The overall generality of this observation is unknown.

Four types of samples are used in this study, including 1) Eosin Y (EOY), a molecular fluorophore with no significant scattering activity; 2) EOY mixed with plain polystyrene

nanoparticles (PSNPs) that are pure scatterers; 3) EOY mixed with dyed PSNP that are scatteringand absorbing-, but not emitting nanoparticles; and 4) fluorescent PSNPs that are comprised of fluorescent dyes impregnated inside PSNPs. The first group of samples are simultaneously light absorbers and emitters with no significant scattering activities, while the remaining three are simultaneous light absorbers, scatterers, and emitters.

The present work focuses on the following three specific objectives. First, we wish to demonstrate the potential pitfalls in UV-vis measurements of fluorescent samples. Part I and II showed how the interference of forward scattered light can cause the experimental UV-vis extinction to deviate from Beer's law even when the sample theoretical extinction is within the LDR of the used UV-vis instrument. Imaginably, forward propagated fluorescence can also cause a similar interference. Second, by using a series of PSNPs with varied sizes and optical properties, we wish to establish a systematical understanding of the effects for light scattering on fluorophore fluorescence intensity and depolarization. Third, we wish to provide a general guideline for experimental investigation on the optical properties of fluorescence nanoparticles that have become increasingly popular in chemical, biological, and materials research. 15-19 There are numerous problematic interpretations of the spectra acquired with these samples, including assigning sample UV-vis extinction spectra as absorbance without considering scattering contribution, and ineffective correction of absorption-IFE on the fluorescence and scattering measurements.²⁰⁻²⁴ Addressing these issues are important for a wide range of scientific inquiries, given the importance of fluorescence in education, research, and technological developments.

EXPERIMENTAL SECTION

Materials and equipment. Polybead carboxylate polystyrene nanoparticles (PSNP), red dyed polystyrene nanoparticles (dPSNP) and fluorescent polystyrene nanoparticles (fPSNP) were purchased from Polysciences, Inc. PSNPs with diameters of 100 nm (Cat #16688-15), 200 nm (Cat #08216-15), and 380 nm PSNP (Cat #21753-15) were abbreviated as PSNP₁₀₀, PSNP₂₀₀, and PSNP₃₈₀, respectively. The dPSNP with a diameter of 530 nm (Cat #19815-15) was abbreviated as dPSNP₅₃₀. fPSNPs with diameters of 43 nm (Cat #16661-10), 95 nm (Cat #17150-10), and 180 nm (Cat #09834-10) were abbreviated as fPSNP₄₃, fPSNP₉₅, and fPSNP₁₈₀, respectively. Analytical grade Eosin Y (EOY) and potassium permanganate (KMnO₄) were obtained from Sigma-Aldrich and used as received without further purification. Nano pure water (18.2 MΩ cm⁻¹, Thermo Scientific) was used for all sample preparations. For simplicity, the EOY and PSNP nanoparticles mixture was abbreviated as EOY/PSNP.

A Shimadzu UV-2600i spectrophotometer with an ISR 2600 integrating-sphere accessory (Duisburg, Germany) was used for all UV-vis and integrating-sphere UV-vis (ISUV) spectra. Fluorescence spectra and the resonance synchronous spectra were obtained using a Fluoromax-4 spectrophotometer (Horiba Jobin Yvon, Edison, NJ USA). A K-Sphere Petite integrating-sphere (Horiba PTI) with an internal diameter of 80 mm and a neutral density filter with an optical density of 2.0 ± 0.05 from 200 to 1100 nm (Thor Labs) was used for all integrating-sphere-assisted resonance synchronous spectroscopy (ISARS) spectral acquisition.

Spectroscopic Measurements: All spectrofluorometer-based spectra were acquired with an integration time of 0.3 seconds and a bandwidth of 2 nm for both excitation and emission monochromators. The G factor spectrum for correcting the polarization bias was quantified in a

previous study.²⁵ All the spectra for the measurements were obtained using a 1 cm Thorlabs UV-fused quartz cuvette with a sample volume of 3 mL at room temperature. A neutral density filter with an optical density of 2.0 ± 0.05 from 200 to 1100 nm (Thor Labs) was used for the fluorescence spectral acquisition of all the EOY samples unless specified.

RESULTS AND DISCUSSION

UV-vis extinction. Part I and Part II showed that forward scattered light can interfere with the UV-vis extinction spectra of scatterer-containing samples.^{1, 2} Such an interference can cause the measured UV-vis intensity to deviate from Beer's law even when the sample theoretical extinctions are within the instrument LDR that is quantified using molecular chromophores. Imaginably, forward fluorescence photons can also reach the UV-vis detector, introducing spectral interference. A generalized model for illustrating how scattering and fluorescence interference can interfere with the UV-vis extinction measurement is developed for analytes that are assumed to be simultaneous scatterers, absorbers, and emitters at the excitation wavelength. In this case, the sample experimental UV-vis extinction intensity $E_{UV}(\lambda_x)$ can be parameterized using Eq. 3. A detailed mathematical derivation is shown in the **Supporting Information**.

$$E_{UV}(\lambda_x) = -\log \frac{I_o(\lambda_x) 10^{-E_T(\lambda_x)} + \eta_s I_{S,fw}(\lambda_x) + \eta_F \int_0^\infty I_{F,fw}(\lambda_x,\lambda_m) d\lambda_m}{I_o(\lambda_x)}$$
(3)

 $E_T(\lambda_x)$ is the theoretical extinction of the sample, which is the sum of sample theoretical absorption and scattering extinction. $I_0(\lambda)$ is the excitation intensity. The integration in the fluorescence term is necessary as the fluorescence emission usually spans a broad wavelength range. Since the conventional UV-vis spectrophotometer uses only excitation wavelengths, with no detection monochromator, fluorescence emission at any wavelength can interfere with UV-vis

measurements. η_S and η_F refer to the fraction of the forward scattered light $I_{S,fw}(\lambda_x)$ and emitted light $\int_0^\infty I_{F,fw}(\lambda_x,\lambda_m)d\lambda_m$, respectively, reaching the UV-vis detector. These values depend on the collection angle of the UV-vis detector and the spatial distribution of the scattered and emitted photons.¹⁴

Eq. 3 can be simplified for predicting the scattering or fluorescence interference with sample UV-vis measurements, including the equations presented in Part I for samples that contain only light scatterers, ¹⁴ and in Part II where analytes are simultaneous absorbers and scatterers. For the simplest fluorescent samples that contain only molecular fluorophores with no significant scattering activities, Eq. 3 is simplified into Eq. 4.

$$E_{UV}(\lambda_x) = -\log \frac{I_0(\lambda_x)10^{-A_T(\lambda_x)} + \eta_F \int_0^\infty I_{F,fw}(\lambda_x,\lambda_m)d\lambda_m}{I_0(\lambda_x)}$$
(4)

We demonstrated earlier that the forward scattered light causes deviation of experimental UV-vis intensity from Beer's law.^{1,2} However, Eq.3 and Eq. 4 show that the forward scattered and fluorescence light also introduce spectral distortion due to the fact that the degree of scattering and fluorescence interference can be strongly wavelength dependent. Such interferences are shown with the extinction spectra acquired with both the conventional UV-vis and recently reported ISUV method for KMnO₄, EOY, and dPSNP₁₈₀ (Figure 1). The experimental UV-vis spectra of KMnO₄ solutions and their corresponding ISUV spectra are the same (Figure 1A-1D). The experimental extinctions are the same as their theoretical extinction intensities for the evaluated wavelengths for the samples with the theoretical extinctions below 4, which is considered the upper LDR limit of the used spectrophotometer. This datum is not surprising because KMnO₄ is approximately a pure light absorber with no significant light scattering. However, the conventional UV-vis spectra and their corresponding ISUV spectra are remarkably

different from both EOY (**Figure 1E-1H**) and fPSNP₁₈₀ (**Figures 1I-1L**)). Nonlinearity appears in the conventional UV-vis measurements even when the theoretical EOY and fPSNP samples are significantly lower than 4. Since EOY differs from KMnO₄ only in the EOY fluorescence activity, the EOY data provide an unequivocal demonstration of the forward fluorescence interference in UV-vis measurement of fluorescent samples.

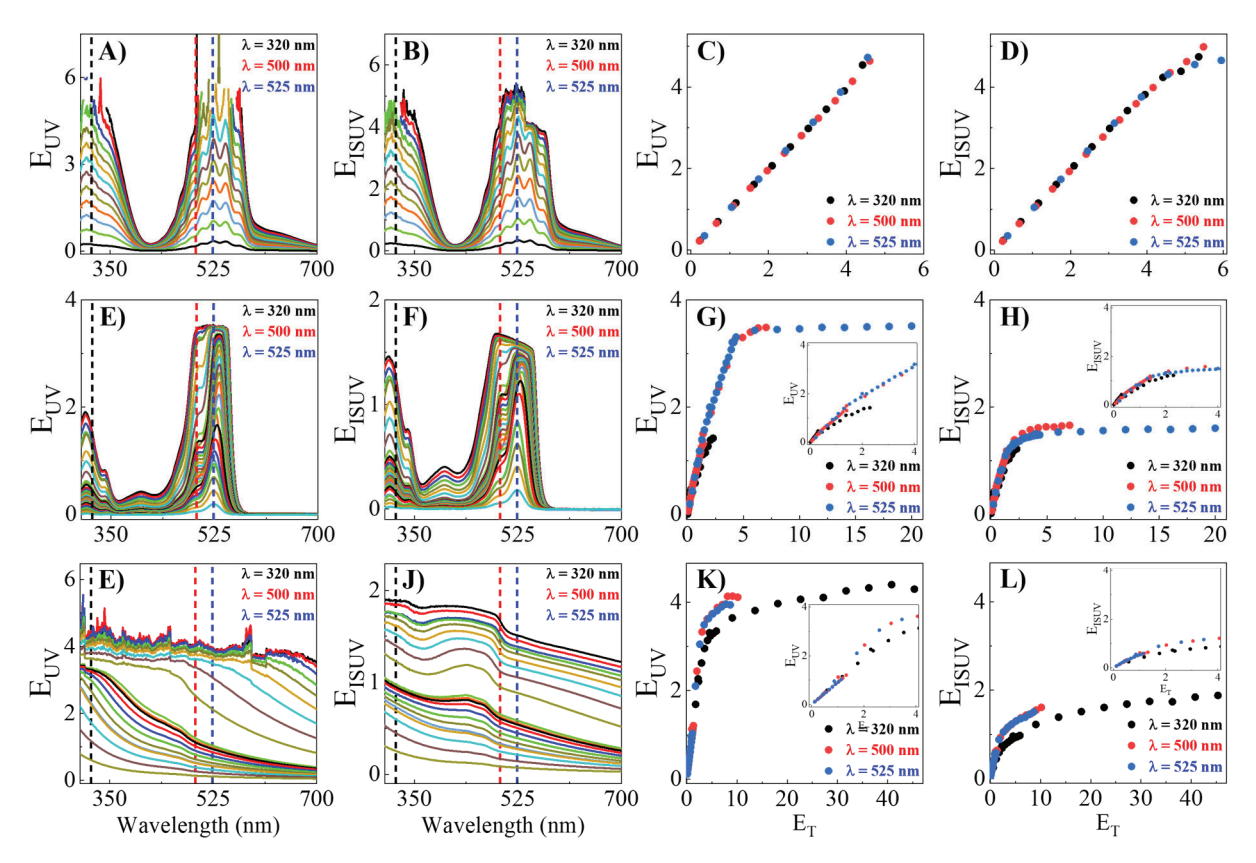


Figure 1. (A, E, I) UV-vis spectra, (B, F, J) ISUV spectra, (C, G, K) UV-vis extinction as a function of the sample theoretical extinction, and (D, H, L) ISUV extinction as a function of the sample theoretical extinction for (A, B, C, D) KMnO₄ from 0.14 to 3.62 mM, (E, F, G, H) EOY from 1.67 to 169.08 μ M in ethanol, and (I, J, K, L) fPSNP₁₈₀ from 0.01 to 1.01 nM. The evaluated wavelengths and the trend lines are color coded. Only the data obtained with a theoretical extinction lower than 4.3 are shown in the trend lines.

The spectral distortion introduced by the scattering and fluorescence interference is shown by comparing the UV-vis spectra obtained from KMnO₄, EOY, and fPSNP₁₈₀, each with two different concentrations (**Figure S1**). The experimental UV-vis of KMnO₄ with different

concentrations differs only in their spectral intensity, provided the extinction spectrum is within the instrument LDR. In contrast, the UV-vis spectra of both EOY and fPSNP exhibit significant spectral distortion that are especially prominent when the measured UV-vis extinction is high. Such spectral distortion can also be seen from the wavelength-dependence of the correlation between the experimental UV-vis extinction and the theoretical extinction of EOY and fPSNP₁₈₀ samples (**Figure 1**).

It is not uncommon that researchers attribute the concentration dependent UV-vis spectra of fluorescent samples to physicochemical interactions among fluorophores or between fluorophores and ligands including nanoscale or larger particles. ²⁶⁻²⁹ Such possibility is excluded in this experiment for the samples used in **Figure 1**. First, the EOY concentration, even in the most concentrated solution, is far below its solubility (1 mg/mL in ethanol). Second, carboxylate fPSNPs used in this work are stable in solutions, and the fluorophore in fPSNP are all impregnated inside a polymer matrix (**Figure S2**). Therefore, the possibility for strong intermolecular interactions in the EOY sample and interparticle interactions in fPSNP₁₈₀ samples should be negligibly small. In other words, the concentration dependence of the EOY and fPSNP UV-vis spectra (**Figure 1**) must be due predominantly to fluorescence and scattering interference. These observations caution the use of UV-vis spectroscopic analysis of fluorescent samples for both fluorophore quantifications and fluorophore interactions because the upper LDR limit for the fluorescent samples can be significantly smaller than the instrument detection limit that is commonly evaluated using molecular chromophores.

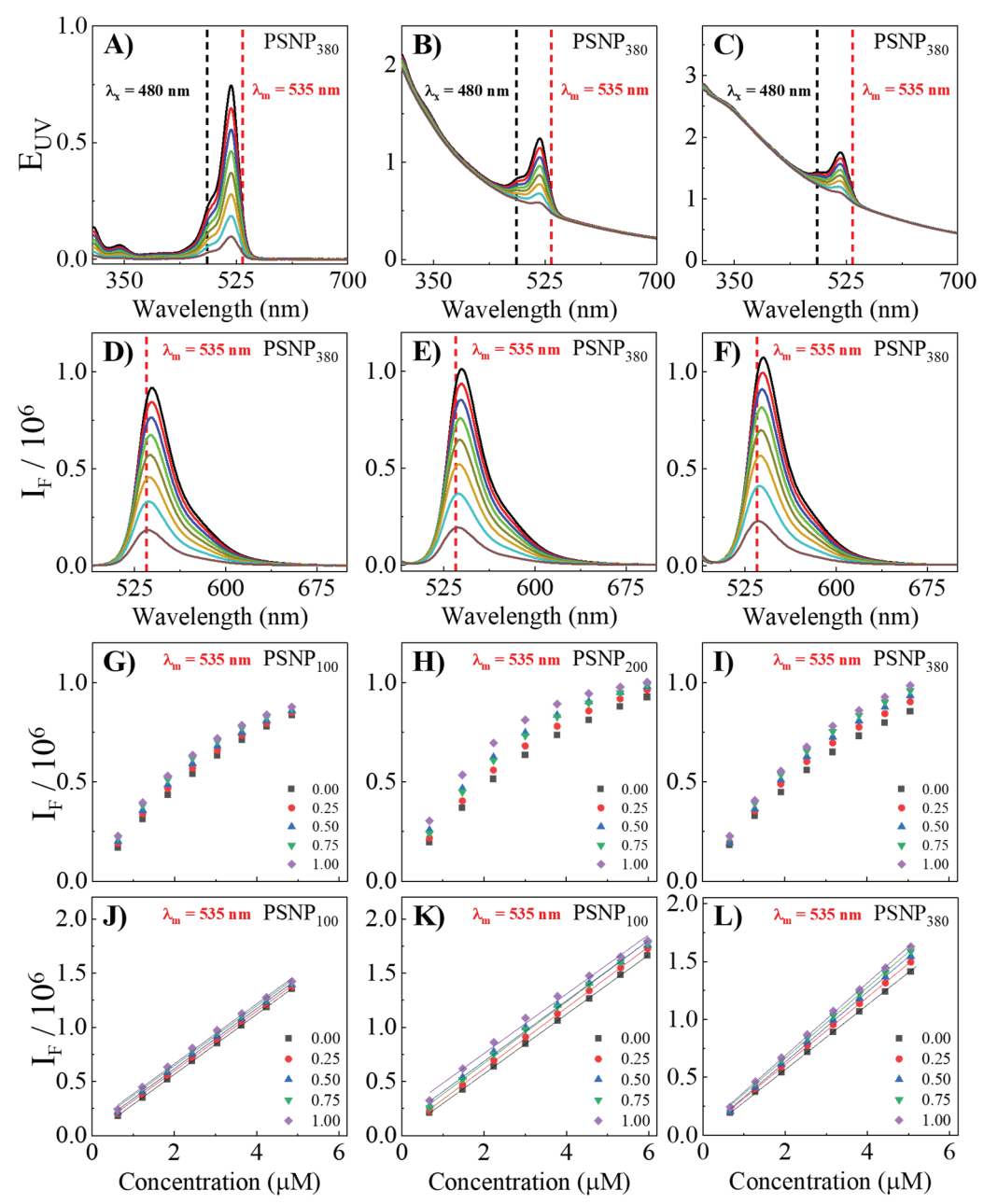


Figure 2. (A-C) UV-vis and (D-F) fluorescence spectra of (A, D) EOY, (B, E) and (C, F) EOY/PSNP₃₈₀ solutions. The PSNP₃₈₀ concentrations for the samples shown in (A, D), (B, E), and (C, F) are 0, 3.83 pM, and 7.69 pM, respectively. The EOY concentrations in each series is the same (0.68, 1.48, 2.23, 3.0, 3.8, 4.6, 5.3, to 6.0 μM). The excitation wavelength is 480 nm for the fluorescence spectra shown. (G-I) as-acquired fluorescence intensity at 535 nm as a function of EOY concentration for EOY/PNSP₁₀₀, EOY/PNSP₂₀₀, and EOY/PSNP₃₈₀, respectively. The legend showed the nominal PSNP scattering extinction in EOY/PSNP solutions. (J-L) Absorption-IFE corrected fluorescence intensity as a function of EOY concentration for the data shown in (G-I). The solid lines shown are obtained by linearly curve fitting. Complete data obtained with EOY/PSNP₁₀₀, EOY/PSNP₂₀₀, EOY/PSNP₃₈₀ are shown in **Figures S3-S5.**

Effect of PSNPs on EOY fluorescence. Plain PSNPs are approximately pure light scatterers with no significant light absorption or emission in the wavelength region of interest; however, one must ensure there is no significant physicochemical interactions between EOY and PSNP before using PSNPs to probe the impact of light scattering on EOY fluorescence. Control experiments reveal that EOY has no significant interactions with dialyzed PSNP₁₀₀, PSNP₂₀₀, or PSNP₃₈₀. The UV-vis spectrum of EOY/PSNP solutions prepared with these PSNPs is approximately the same as the sum of UV-vis spectra acquired with their respective PSNP and EOY controls. In contrast, there is a significant difference between the experimental EOY/PSNP₅₀ UV-vis spectrum and the mathematical sum of the UV-vis spectrum of the EOY and dialyzed PSNP₅₀ controls (**Figure S6**). It is noted that the maximum UV-vis extinctions for all explored samples (Figure 2, Figure S3-S5) are kept below 2 at 520 nm, the peak EOY absorption wavelength. In this case, the interference of forward scattered or forward fluorescence light to the sample UV-vis measurement should be negligibly small (Figure 1). Therefore, the difference between the experimental UV-vis spectrum of the PSNP₅₀/EOY mixture solution and the sum spectrum of the PSNP₅₀ and EOY controls is a definitive marker of EOY and PSNP₅₀ interaction with the dialyzed PSNP₅₀. To avoid data misinterpretation, the effects of light scattering on fluorophore fluorescence were only investigated with PSNP₁₀₀, PSNP₂₀₀, and PSNP₃₈₀ (**Figure 2**), but not PSNP₅₀.

Figure 2 shows three series of example UV-vis extinction spectra (Figure 2A-2C) and fluorescence emission spectra (Figures 2D-2F)) obtained with EOY and EOY/PSNP₃₈₀. Complete sets of UV-vis and fluorescence emission spectra for all EOY/PSNP samples summarized in Figure 2J-2L are provided in the supporting information (Figures S3-S5). The as-acquired EOY fluorescence exhibits poor linearity with the EOY concentration (Figure 2G-2I) in EOY controls and all EOY/PSNP solutions. Empirically, however such nonlinearity can all be corrected by

applying the absorption-IFE model (Eq. 2), where A_x and A_m used for the absorption-IFE correction are the EOY absorbance at the excitation and emission wavelengths, respectively. The d_x and d_m are 0.49 and 0.52, respectively, these values were determined using a water Raman method.⁸ Indeed, the absorption-IFE-corrected fluorescence intensities (**Figure 2J-2L**) all exhibit excellent linearity with EOY concentration in both EOY and EOY/PSNP solutions.

Cross examination of the linearly fitting equations in **Figure 2J-2L** are revealing. Evidently increasing PSNP₁₀₀ and PSNP₂₀₀ concentration increases only the intercept of the linearly fitted equation but has no significant effect on the slope of the linear equations. This indicates that the presence of PSNP₁₀₀ or PSNP₂₀₀ in the EOY solution have no significant impact on fluorophore emission intensity. However, the intercept of these linear equations increases with increasing PSNP₁₀₀ or PSNP₂₀₀ concentration. This is likely due to PSNP background interferences (**Figure S7**).

Increasing PSNP₃₈₀ concentration increases both the intercepts and slopes of the linear equation obtained for the PSNP₃₈₀/EOY solutions. The enhancement of the intercept is, again, likely due to the PSNP background. However, the increased slopes indicate the PSNP₃₈₀ scattering enhances the EOY fluorescence emission. Collectively, the data obtained with PSNP₁₀₀, PSNP₂₀₀, and PSNP₃₈₀ strongly suggest that only the light scattering by large PSNPs have a significant impact on fluorophore fluorescence. In contrast, the scattering by PSNPs of 200 nm or smaller in diameter have a negligibly small impact on the fluorophore fluorescence emission. This conclusion is also supported by the earlier report that light scattering by 100 nm PSNPs did not have a significant effect on the fluorescence intensity of fluorescent quantum dots,⁹ as well as the fPSNPs obtained in this work (*vide infra*). This fluorescence enhancement by large PSNPs is also

consistent with the experimental data obtained with dPSNPs with a nominal diameter of 530 nm (vide infra).

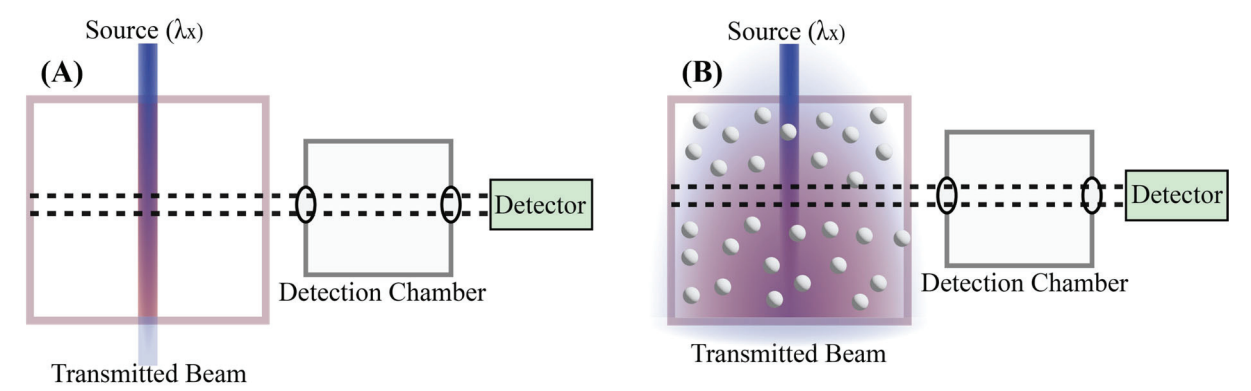


Figure 3: Schematic representation of pin-hole effects in (A) scattering-free, and (B) scatterer-containing fluorescent samples. The incident and scattered light are in blue, and emitted light is in red. The black dashed region represents the region where fluorescence photons are most effectively collected due to the instrument pin-hole effect.

$$I(\lambda_x, \lambda_m) = I(\lambda_x)Q(\lambda_x, \lambda_m)R(\lambda_m)l_s A_{x,f} 10^{-(A_{x,S}d_x + A_{m,S}d_m)}$$
(5)

Mechanistically, the effect of light scattering on fluorophore fluorescence explained by visiting a first-principles model we developed recently for correlating fluorophore fluorescence $I(\lambda_x, \lambda_m)$ acquired with a conventional spectrofluorometer (Eq. 5) for scattering-free fluorescence samples.⁷ $I(\lambda_x)$ represents the excitation intensity, $A_{x,s}$ and $A_{m,s}$ are sample light absorbance at the excitation and emission wavelengths, respectively. For samples that contains only the molecular fluorophores, $A_{x,s}$ and $A_{m,s}$ are equivalent to $A_{x,f}$ and $A_{m,f}$, respectively. $A_{x,f}$ stands for the fluorophore absorbance at the excitation wavelength. $Q(\lambda_x, \lambda_m)$ represents the quantum yield of the fluorophore at the specified excitation and emission wavelength. $R(\lambda_m)$ summarizes the instrument responsivity in detection of emitted photons. l_s is the effective sampling path length. Due to the instrument pinhole effect, shown schematically in **Figure 3**, only the fluorescence signal generated within this effective sampling path length contributes significantly

to the experimental fluorescence spectrum.⁷ The effective sampling volume for scatterer-free solutions must be smaller than that for scatterer-containing samples due to the scattering diversity of the optical path from the otherwise collimated beam (Figure 3). This enhancement of the effective sampling volume can also be viewed as the enhancement of absorption path length enhancement for excitation photons entering the effective sampling path length l_s . For the scatterer-free sample, the effective absorption path length is equal to the effective sampling path length l_s . However, for scatterer-containing samples, the effective absorption path length is $k_s l_s$ where $k_s \ge 1$.

The net effect of light scattering on fluorescence depends on two competing factors: the absorption pathlength inside the sampling volume that increase the possibility of the excitation to generate fluorescence emission, and the scattering-IFE that reduces the number of photons entering the sampling volume. Such scattering-IFE has been shown in Part I of this series of companion articles and is manifested by both scattering extinction and intensity measurements. It is emphasized that scattering-IFE is extraordinarily complex and it depends on not only the sample scattering extinction, but also its scattering depolarization. Compared to the absorption-IFE, however, scattering-IFE is drastically smaller. Herein we use η_S to present the scattering-IFE scattering on the fluorophore fluorescence.

Eq. 6 represents the revised model for scatterer-containing fluorescent samples. The only difference between Eq. 6 and Eq. 5 is the k_S and η_S terms discussed in the preceding sections.

$$I(\lambda_x, \lambda_m) = I(\lambda_x)Q(\lambda_x, \lambda_m)R(\lambda_m)k_S l_s A_{x,f} 10^{-(A_{x,S}d_x + A_{m,S}d_m) - \eta_S}$$
(6)

Under the condition where scattering-IFE is small ($\eta_S < 0.05$), Eq. 6 can be simplified into Eq. 7 where β_S is the scatterer-dependent constant. This constant can also be viewed as a

scattering-dependent correction factor for the light absorption inside the effective sampling volume.

$$I(\lambda_x, \lambda_m) = I(\lambda_x)Q(\lambda_x, \lambda_m)R(\lambda_m)\beta_s l_s A_{x,f} 10^{-(A_{x,s}d_x + A_{m,s}d_m)}$$
(7)

Combining Eq. 2 and Eq. 7 leads to Eq. 8, showing that the absorption-IFE corrected fluorescence intensity is linearly correlated with the fluorophore absorbance $A_{x,f}$, and to Eq. 9 by replacing $A_{x,f}$ with the fluorophore concentration using Beer's law and using $K(\lambda_m)$ as $R(\lambda_m)\varepsilon_f b$

$$I^{corr}(\lambda_x, \lambda_m) = I(\lambda_x)Q(\lambda_x, \lambda_m)R(\lambda_m)\beta_s l_s C_f$$
 (8)

$$I^{corr}(\lambda_x, \lambda_m) = I(\lambda_x)Q(\lambda_x, \lambda_m)K(\lambda_m)\beta_s l_s C_f$$
(9)

The near perfect linearity of the experimental data obtained with EOY/PSNP provides empirical validation of Eq. 9 for correlating sample fluorescence intensity with fluorophore concentration. Therefore, Eq. 9 is a generalized model for correlating the sample fluorescence and fluorophore concentration in solutions containing both absorption and scatterers. β_S is approximately 1 for EOY mixed with both PSNP100 (**Figure 2J**) and PSNP200 (**Figure 2K**), indicating that the two competing factors by light scattering on EOY fluorescence cancel each other. This conclusion is consistent with our earlier report that the scattering by PSNP100 has no significant impact on quantum dots fluorescence. However, β_S value is invariably larger than 1 for EOY/PSNP380, and it increases with increasing PSNP380 scattering extinction (**Figure 2L**). This observation indicates the absorption path length enhancement by PSNP380 is more significant than its scattering-IFE. This result is consistent with the fact that the scattering-IFE is much more significant for PSNP100 and PSNP200 than that for PSNP380. The fact that light absorption and scattering can both change fluorophore fluorescence with totally different ways (attenuate or enhance) demonstrates the complexity of fluorescence spectroscopic analysis of turbid samples.

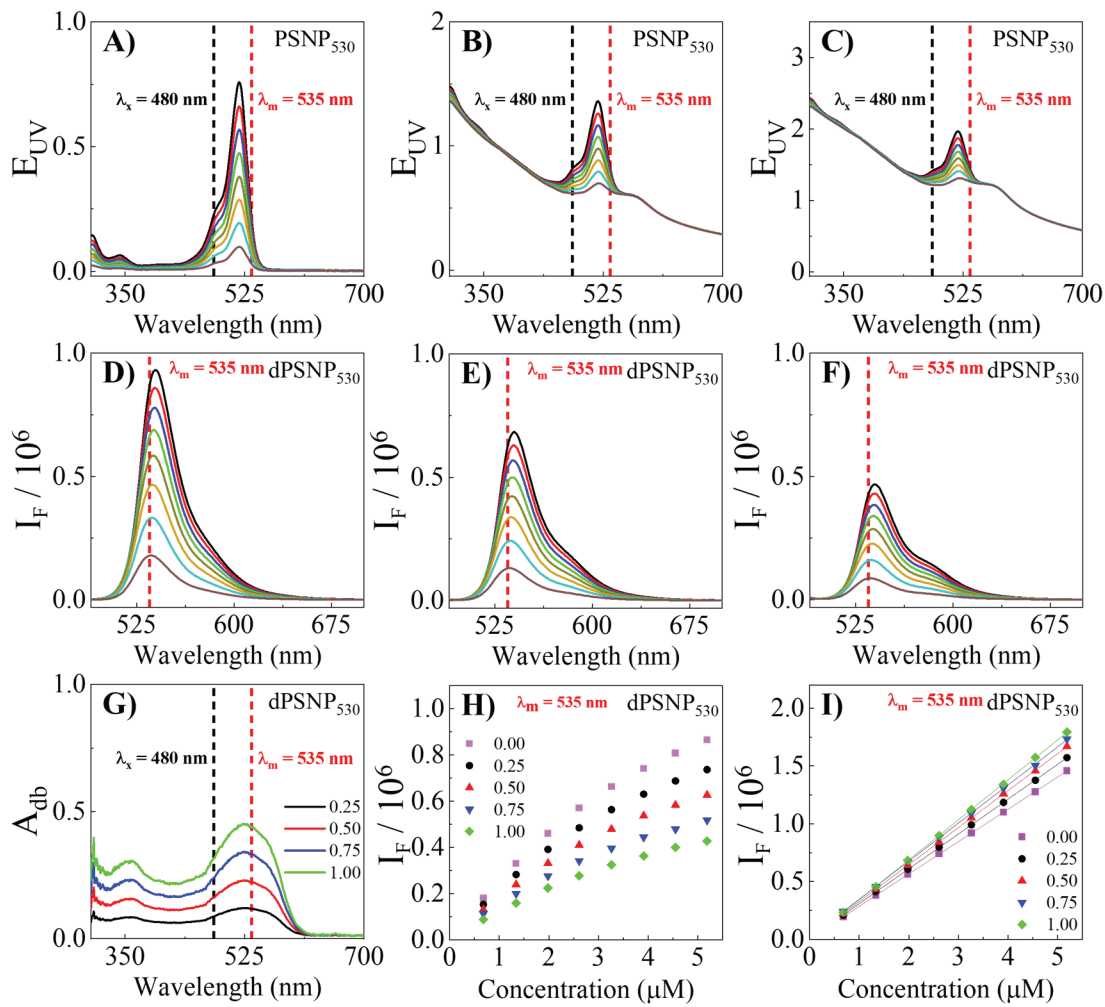


Figure 4. (A-C) UV-vis and (D-F) fluorescence spectra of (A, D) EOY, (B, E) and (C, F) EOY/dPSNP₅₃₀. The PSNP₅₃₀ concentration for samples used in (A, D), (B, E), and (C, F) are 0, 1.18 pM, and 2.31 pM, respectively. The EOY concentrations in the sample series are all the same, and range from 0.68 to 5.19 μM. The excitation wavelength is 480 nm for the fluorescence spectra shown. (G) ISARS-derived double-beam absorbance for dPSNP₅₃₀ used for the EOY/dPSNP₅₃₀ solutions. (H, I) as-acquired and absorption-IFE corrected fluorescence intensity as a function of EOY concentration. Complete data for all EOY/dPSNP₅₃₀ solutions are shown in **Figure S8**.

Effect of dPSNP on EOY fluorescence. The dPSNP₅₃₀ used in this work are simultaneous light absorbers and scatterers with no significant fluorescence activities.² The as-acquired EOY fluorescence decreases with increasing dPSNP₅₃₀ concentration (**Figure 4A-4F, 4H**). After correcting the absorption-IFE on EOY fluorescence, however, EOY fluorescence increases with increasing dPSNP₅₃₀ concentrations (**Figure 4I**). This observation indicates, while the dPSNP₅₃₀

light absorption reduces EOY fluorescence, its scattering enhances the fluorescence intensity. It is noted that the $A_{x,s}$ and $A_{m,s}$ values used for absorption IFE correction are the sum of the EOY and dPSNP absorbance at the excitation and the emission wavelengths, respectively. Therefore, one must obtain the dPSNP absorbance spectra (**Figure 4G**) before the absorption-IFE correction. The experimental separation of dPSNP extinction spectrum into its absorption and extinction component spectra was recently reported in Part II.²

The data obtained with the dPSNP allow us to make a head-to-head comparison of the impact of light absorption and scattering on fluorophore fluorescence. dPSNP₅₃₀ is primarily a light scatterer at the excitation wavelength (480 nm) (**Figure 4**). Its absorption extinction to scattering extinction ratio at 480 nm is 0.3436. However, the overall effects of dPSNP on the asacquired EOY fluorescence are dominated by its light absorption. The impact of the light scattering by dPSNP₅₃₀ is evident only in the absorption-IFE corrected spectra. This highlights the importance of separating sample absorption and scattering in discussion of the sample UV-vis extinction of fluorescence measurements. Unfortunately, in current literature, the impacts of sample light scattering and absorption on fluorescence measurements have either not been considered at all, or their impacts have been assumed to be the same by using UV-vis extinction for sample IFE correction.³¹⁻³⁵

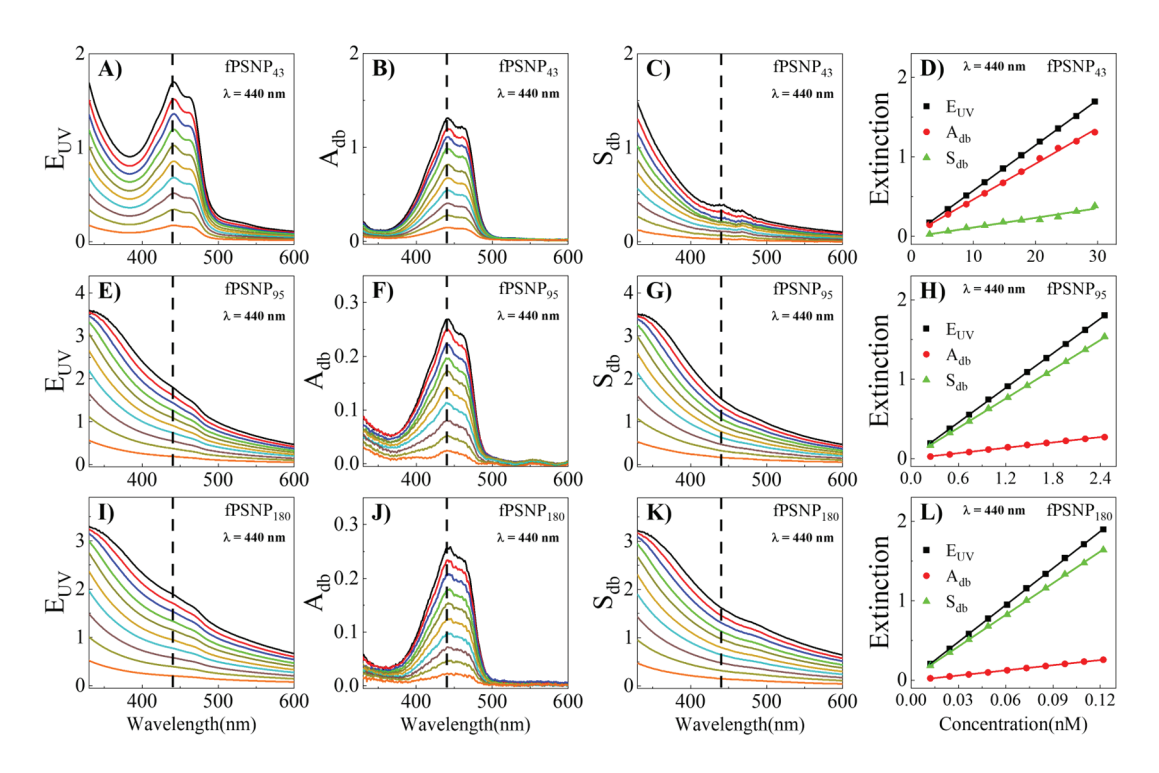


Figure 5. (A, E, I) experimental extinction spectra of fPSNP₄₃, fPSNP₉₅, fPSNP₁₈₀, respectively. (B, F, J) UV-vis absorption extinction spectra derived from ISARS-based absorbance spectra for the samples shown in (A), (E), (I), respectively. (C, G, K) UV-vis scattering extinction spectra of fPSNP₄₃, fPSNP₉₅, fPSNP₁₈₀ samples, which were obtained by subtracting the experimental extinction spectrum in (A, E, I) by the corresponding absorption extinction spectrum in (B, F, J), respectively. (D, H, L) UV-vis total extinction, absorption extinction, and scattering extinction intensity at 440 nm for the fPSNP₄₃, fPSNP₉₅, fPSNP₁₈₀, respectively.

Optical properties of fPSNPs: fPSNPs are made with molecular fluorophores dispersed in polystyrene matrix. They are simultaneous light absorbers, scatterers, and emitters at the wavelength where fPSNP absorbs. While the PSNP matrix is approximately pure scatterers, quantification of the absorption and fluorescence activities of the impregnated fluorophores, to our knowledge, are not available.

Experimental separation of light scattering and absorption contribution to fPSNP UV-vis extinction spectra (**Figure 5**) is performed using the recent ISARS method.^{2, 36} The complete datasets for the as-acquired ISARS intensity spectra, ISARS-based absorbance, and the ISARS-derived double-beam absorbance spectra are shown in the supporting information (**Figure S9**-

S10). The effectiveness of ISARS for quantification of sample absorption and scattering extinction is shown by the near perfect linear dependence of experimental total extinction, absorption extinction, and scattering extinction on the fPSNP concentration (**Figure 5D, 5H, 5L**). It is noted that, to avoid the interference of forward scattered light in the UV-vis spectral measurement, the UV-vis extinction intensities of all fPSNP solutions were all kept below 2 at the excitation wavelength.

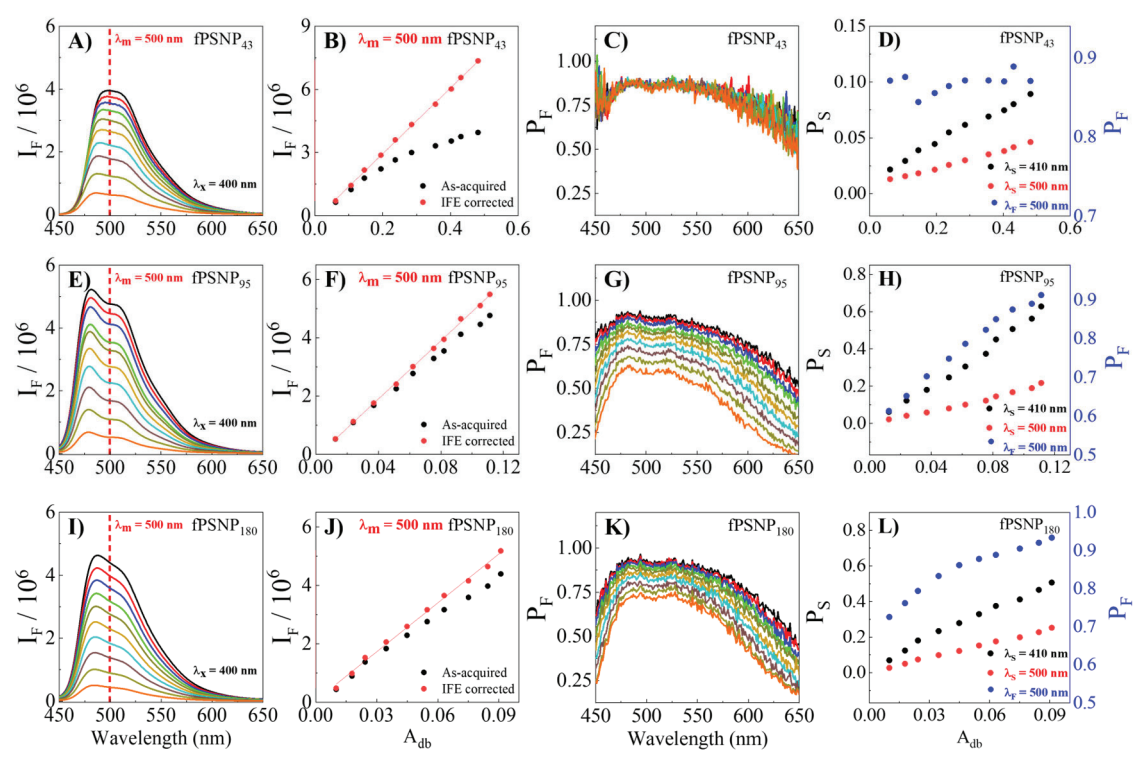


Figure 6. (A, E, I) Fluorescence emission spectra of fPSNP₄₃, fPSNP₉₅, fPSNP₁₈₀, respectively. (B, F, J) (Black dots) As-acquired and (red dots) absorption-IFE corrected fluorescence intensity as a function of fPSNP₄₃, fPSNP₉₅, fPSNP₁₈₀ absorption extinction at the excitation wavelength. (C, G, K) Fluorescence emission depolarization spectra of the fPSNP₄₃, fPSNP₉₅, fPSNP₁₈₀ samples. (D, H, L) Scattering depolarization at 400 nm and 500 nm and fluorescence depolarization at 500 nm as a function of the fPSNP scattering extinction at the excitation wavelength. The as-acquired linearly polarized spectra for light scattering and fluorescence depolarization quantification are shown in **Figure S11-S12**.

The UV-vis extinction spectra of the fPSNPs (Figure 5A, 5E, and 5I) are different, which is not surprising due to the strong size dependence of light scattering. However, the absorbance

spectra (Figure 5B, 5F, and 5J) of the fPSNPs of three different sizes bear high similarity, which is consistent with the fact that the fluorophore inside these fPSNPs are the same according to the vendor. By assuming that the absorption activities of the fluorophore imbedded inside fPSNPs are the same, we estimate both the relative fluorophore-to-fPSNP number ratio and the fluorophore volume density in the polystyrene matrix for fPSNP of difference sizes. The relative fluorophore-to-fPSNP number ratio is 1, 2.4, and 42.6 for fPSNP43, fPSNP95, fPSNP180, respectively, while their relative fluorophore volume density is 1, 0.22, and 0.58. In other words, the fluorophores are most densely packed inside fPSNP43.

In contrast to the high similarity of the UV-vis absorption extinction spectra among fPSNP₄₃, fPSNP₉₅, and PSNP₁₈₀, the shape of the emission spectra for these fPSNPs are somewhat different, specifically between the fPSNP₄₃ spectrum and those of fPSNP₉₅ and PSNP₁₈₀. Further, the fluorescence activity of the fluorophore insides fPSNP₄₃ is also significantly different from those inside fPSNP₉₅ and fPSNP₁₈₀ (Figure 6A, 6B, 6E, 6F, 6I and 6J). The quantum yield of the fluorophore inside PSNP matrix is proportional to the slope of the linear curve between the absorption-IFE corrected fluorescence intensity and fluorophore absorbance at the excitation wavelength (Eq. 8). The relative fluorescence activities of the fPSNP₉₅ and fPSNP₁₈₀ are very similar and they are ~1.8 times higher than that of fPSNP₄₃. One likely reason in the fluorescence activity differences is that the fluorophores packing density inside fPSNP₄₃ is too high. When the intermolecular distance is shorter than a certain threshold volume, the fluorophore fluorescence activities decreases because dipole-dipole interactions among the neighboring fluorophores enhance nonradiative decays of the excited fluorophores.³⁷⁻⁴⁰

Cascading light scattering can enhance both scattering and fluorescence depolarizations. Such an effect is especially evident for fPSNP₉₅ and fPSNP₁₈₀. The fPSNP₄₃, fPSNP₉₅, and

fPSNP₁₈₀ scattering depolarization spectra are quantified using the linearly polarized resonance spectroscopic method, while the fPSNP₄₃, fPSNP₉₅, fPSNP₁₈₀ fluorescence depolarization spectra (Figure 6C, 6J, 6K) are acquired using linearly polarized fluorescence measurements.^{12, 41} Mechanistically, the fluorescence depolarization increase with fPSNP concentration is due to multiple combined effects. Firstly, the depolarization increases with increasing scatterers' concentration. Any fluorescence generated by absorbing scattered light the scattering of emitted photons enhances fluorescence depolarizations. Secondly, any cascading fluorophore absorption, emission, reabsorption, and reemission process will increase the fluorescence depolarization. The depolarization of the re-emitted photons must be higher than the initial emitted photons.

CONCLUSIONS

The current work focuses on cascading optical processes and their impacts on spectroscopic characterization of fluorescence samples. A generalized model is developed for mechanistic understanding on how forward scattered and emitted light interferes with UV-vis measurement to deviate from Beer's law and causes spectral distortions of fluorescence and/or scattering samples. The interplay among absorption, scattering, and fluorescence emission is explored through three sets of samples, including a mixture of a fluorophore and PSNPs, a mixture of a fluorophore with dyed PSNPs, and fluorescence nanoparticles that act as simultaneous absorbers, scatterers, and emitters. The absorption-IFE corrected fluorophore fluorescence all exhibited excellent linearity with the fluorophore absorbance (or equivalently, to the fluorophore concentration). While the light absorption by the nonfluorogenic dye invariably reduces the sample fluorescence by exerting the absorption-IFE, the impact of light scattering on the fluorophore fluorescence depends on two competing factors: the scattering-IFE that reduces the

fluorescence intensity, the absorption path length enhancement inside the effective sampling

volume that can enhance fluorescence emission. The combined ISARS, LRPS, and fluorescence

measurements enabled the experimental quantification of the UV-vis absorption, scattering, and

fluorescence activities of fluorescence nanoparticles. These spectroscopic data also allowed the

quantification of the scattering and fluorescence depolarizations as a function of the concentration

of fluorescent nanoparticles. Although it is expected that the findings of this study will be

applicable to all relatively low optical light fluorescent samples with an optical density of 2 or less,

further studies will be needed to determine their relevance for optically dense samples.

ASSOCIATED CONTENT

Supporting information

Derivation of Eq. 3; Completed UV-vis and emission spectra of EOY/PSNP and EOY/dPSNP

solutions; PSNP fluorescence background spectrum; ISARS analysis of fPSNPs.

AUTHOR INFORMATION

Corresponding Authors

Dongmao Zhang, E-mail: <u>Dongmao@chemistry.msstate.edu</u>

Notes

The authors declare no competing financial interest.

Acknowledgement

This work was supported in part by the Center of Biomedical Research Excellence Program funded through the Center for Research Capacity Building in the National Institute for General Medical

24

Sciences (P20GM103646), and by an NSF Grant (CHE 2203571). SZ is grateful for the support from NSF (DMR- 2004546) and the Extreme Science and Engineering Discovery Environment (XSEDE) as the service provider through allocation to szou. The content is solely the responsibility of the authors and does not necessarily represent the official views of the National Institutes of Health or National Science Foundation.

References:

- 1. Nawalage, S.; Wathudura, P.; Wang, A.; Wamsley, M.; Zou, S.; Zhang, D., Effects of Cascading Optical Processes: Part I: Impacts on Quantification of Sample Scattering Extinction, Intensity, and Depolarization. *Analytical Chemistry* **2023**, *ASAP*.
- 2. Wathudura, P.; Wamsley, M.; Wang, A.; Chen, K.; Nawalage, S.; Wang, H.; Zou, S.; Zhang, D., Effects of cascading optical processes. Part II: Impacts on experimental quantification of sample absorption and scattering properties. *Analytical Chemistry* **2023**, *ASAP*.
- 3. Soos, M.; Lattuada, M.; Sefcik, J., Interpretation of Light Scattering and Turbidity Measurements in Aggregated Systems: Effect of Intra-Cluster Multiple-Light Scattering. *The Journal of Physical Chemistry B* **2009**, *113* (45), 14962-14970.
- 4. Oelkrug, D.; Brun, M.; Rebner, K.; Boldrini, B.; Kessler, R., Penetration of light into multiple scattering media: model calculations and reflectance experiments. Part I: the axial transfer. *Applied Spectroscopy* **2012**, *66* (8), 934-43.
- 5. Lakowicz, J. R., *Principles of fluorescence spectroscopy*. Springer: 2006.
- 6. Valeur, B.; Berberan-Santos, M. N., *Molecular Fluorescence: Principles and Applications*. 2nd ed.; Wiley-VCH Verlag GmbH & Co. KGaA: 2012.
- 7. Wamsley, M.; Nawalage, S.; Hu, J.; Collier, W. E.; Zhang, D., Back to the Drawing Board: A Unifying First-Principle Model for Correlating Sample UV–Vis Absorption and Fluorescence Emission. *Analytical Chemistry* **2022**, *94* (19), 7123-7131.
- 8. Nettles, C. B., II; Hu, J.; Zhang, D., Using Water Raman Intensities To Determine the Effective Excitation and Emission Path Lengths of Fluorophotometers for Correcting Fluorescence Inner Filter Effect. *Analytical Chemistry* **2015**, *87* (9), 4917-4924.
- 9. Xu, J. X.; Vithanage, B. C. N.; Athukorale, S. A.; Zhang, D., Scattering and absorption differ drastically in their inner filter effects on fluorescence, resonance synchronous, and polarized resonance synchronous spectroscopic measurements. *Analyst* **2018**, *143* (14), 3382-3389.
- 10. Leese, R. A.; Wehry, E. L., Corrections for inner-filter effects in fluorescence quenching measurements via right-angle and front-surface illumination. *Analytical Chemistry* **1978**, *50* (8), 1193-1197.
- 11. Siano, S. A., Deconvolution of multicomponent fluorescence spectra in the presence of absorption inner-filter effects. *Journal of Quantitative Spectroscopy and Radiative Transfer* **1992,** 47 (1), 55-73.
- 12. Xu, J. X.; Siriwardana, K.; Zhou, Y.; Zou, S.; Zhang, D., Quantification of Gold Nanoparticle Ultraviolet–Visible Extinction, Absorption, and Scattering Cross-Section Spectra and Scattering Depolarization Spectra: The Effects of Nanoparticle Geometry, Solvent Composition, Ligand Functionalization, and Nanoparticle Aggregation. *Analytical Chemistry* **2018**, *90* (1), 785-793.
- 13. Xu, J. X.; Hu, J.; Zhang, D., Quantification of Material Fluorescence and Light Scattering Cross Sections Using Ratiometric Bandwidth-Varied Polarized Resonance Synchronous Spectroscopy. *Analytical Chemistry* **2018**, *90* (12), 7406-7414.

- 14. Nawalage, S.; Wathudura, P.; Wang, A.; Wamsley, M.; Zou, S.; Zhang, D., Effects of Cascading Optical Processes: Part I: Impacts on Quantification of Sample Scattering Extinction, Intensity, and Depolarization. *Analytical Chemistry* **2023**.
- 15. Kong, J.; Zhang, J.; Wang, Y.; Qi, W.; Rao, H.; Hu, L.; Su, R.; He, Z., Bioinspired pH-Sensitive Fluorescent Peptidyl Nanoparticles for Cell Imaging. *ACS Applied Materials & Interfaces* **2020**, *12* (4), 4212-4220.
- 16. Han, Y.; Lv, W.; Chen, H.; Li, H.; Chen, J.; Li, Z.; Qiu, H., Chiral Fluorescent Silicon Nanoparticles for Aminopropanol Enantiomer: Fluorescence Discrimination and Mechanism Identification. *Analytical Chemistry* **2020**, *92* (5), 3949-3957.
- 17. Saladino, G. M.; Vogt, C.; Li, Y.; Shaker, K.; Brodin, B.; Svenda, M.; Hertz, H. M.; Toprak, M. S., Optical and X-ray Fluorescent Nanoparticles for Dual Mode Bioimaging. *ACS Nano* **2021**, *15* (3), 5077-5085.
- 18. Ong, S. Y.; Zhang, C.; Dong, X.; Yao, S. Q., Recent Advances in Polymeric Nanoparticles for Enhanced Fluorescence and Photoacoustic Imaging. **2021**, *60* (33), 17797-17809.
- 19. Li, W.; Kaminski Schierle, G. S.; Lei, B.; Liu, Y.; Kaminski, C. F., Fluorescent Nanoparticles for Super-Resolution Imaging. *Chemical Reviews* **2022**, *122* (15), 12495-12543.
- 20. Pahari, S. K.; Olszakier, S.; Kahn, I.; Amirav, L., Magneto-Fluorescent Yolk-Shell Nanoparticles. *Chemistry of Materials* **2018**, *30* (3), 775-780.
- 21. Zhu, Z.; Tian, D.; Gao, P.; Wang, K.; Li, Y.; Shu, X.; Zhu, J.; Zhao, Q., Cell-Penetrating Peptides Transport Noncovalently Linked Thermally Activated Delayed Fluorescence Nanoparticles for Time-Resolved Luminescence Imaging. *Journal of the American Chemical Society* **2018**, *140* (50), 17484-17491.
- 22. Caponetti, V.; Trzcinski, J. W.; Cantelli, A.; Tavano, R.; Papini, E.; Mancin, F.; Montalti, M., Self-Assembled Biocompatible Fluorescent Nanoparticles for Bioimaging. **2019**, *7*.
- 23. Fang, Y.; Xing, C.; Zhan, S.; Zhao, M.; Li, M.; Liu, H.; Wang, C., Multifunctional Magnetic–Fluorescent Nanoparticle: Fabrication, Bioimaging, and Potential Antibacterial Applications. *ACS Biomaterials Science & Engineering* **2019**, *5* (12), 6779-6793.
- 24. Zhang, J.; Fang, F.; Liu, B.; Tan, J.-H.; Chen, W.-C.; Zhu, Z.; Yuan, Y.; Wan, Y.; Cui, X.; Li, S.; Tong, Q.-X.; Zhao, J.; Meng, X.-M.; Lee, C.-S., Intrinsically Cancer-Mitochondria-Targeted Thermally Activated Delayed Fluorescence Nanoparticles for Two-Photon-Activated Fluorescence Imaging and Photodynamic Therapy. *ACS Applied Materials & Interfaces* **2019**, *11* (44), 41051-41061.
- 25. Zhao, Y.; Hu, Y.; Zhong, Y.; Wang, J.; Liu, Z.; Bai, F.; Zhang, D., Missing Links between the Structures and Optical Properties of Porphyrin Assemblies. *The Journal of Physical Chemistry C* **2021**, *125* (40), 22318-22327.
- 26. Nagai, A.; Miyake, J.; Kokado, K.; Nagata, Y.; Chujo, Y., Highly Luminescent BODIPY-Based Organoboron Polymer Exhibiting Supramolecular Self-Assemble Structure. *Journal of the American Chemical Society* **2008**, *130* (46), 15276-15278.
- 27. Choi, Y.-J.; Luo, T.-J. M., Self-Assembly of Silver—Aminosilica Nanocomposites through Silver Nanoparticle Fusion on Hydrophobic Surfaces. *ACS Applied Materials & Interfaces* **2009**, *1* (12), 2778-2784.
- 28. Santos, P. J.; Macfarlane, R. J., Reinforcing Supramolecular Bonding with Magnetic Dipole Interactions to Assemble Dynamic Nanoparticle Superlattices. *Journal of the American Chemical Society* **2020**, *142* (3), 1170-1174.

- 29. Wang, J.; Zhang, C.; Liu, Z.; Li, S.; Ma, P.; Gao, F., Target-Triggered Nanomaterial Self-Assembly Induced Electromagnetic Hot-Spot Generation for SERS–Fluorescence Dual-Mode In Situ Monitoring MiRNA-Guided Phototherapy. *Analytical Chemistry* **2021**, *93* (41), 13755-13764.
- 30. Sigma-Aldrich Eosin Y. https://www.sigmaaldrich.com/US/en/product/sial/e4009 (accessed 02/07/2023).
- 31. Pan, D.; Liang, P.; Zhong, X.; Wang, D.; Cao, H.; Wang, W.; He, W.; Yang, Z.; Dong, X., Self-Assembled Porphyrin-Based Nanoparticles with Enhanced Near-Infrared Absorbance for Fluorescence Imaging and Cancer Photodynamic Therapy. *ACS Applied Bio Materials* **2019**, *2* (3), 999-1005.
- 32. Kharey, P.; Dutta, S. B.; M, M.; Palani, I. A.; Majumder, S. K.; Gupta, S., Green synthesis of near-infrared absorbing eugenate capped iron oxide nanoparticles for photothermal application. *Nanotechnology* **2020**, *31* (9), 095705.
- 33. Zhang, W.; Li, Y.; Xu, L.; Wang, D.; Long, J.; Zhang, M.; Wang, Y.; Lai, Y.; Liang, X.-J., Near-Infrared-Absorbing Conjugated Polymer Nanoparticles Loaded with Doxorubicin for Combinatorial Photothermal-Chemotherapy of Cancer. *ACS Applied Polymer Materials* **2020**, *2* (10), 4180-4187.
- 34. Siddiquee, S.; Saallah, S.; Bohari, N. A.; Ringgit, G.; Roslan, J.; Naher, L.; Hasan Nudin, N. F. Visual and Optical Absorbance Detection of Melamine in Milk by Melamine-Induced Aggregation of Gold Nanoparticles *Nanomaterials* [Online], 2021.
- 35. Zhu, Y.; Wang, Z.; Zhao, R.; Zhou, Y.; Feng, L.; Gai, S.; Yang, P., Pt Decorated Ti3C2Tx MXene with NIR-II Light Amplified Nanozyme Catalytic Activity for Efficient Phototheranostics. *ACS Nano* **2022**, *16* (2), 3105-3118.
- 36. Wamsley, M.; Wathudura, P.; Hu, J.; Zhang, D., Integrating-Sphere-Assisted Resonance Synchronous Spectroscopy for the Quantification of Material Double-Beam UV–Vis Absorption and Scattering Extinction. *Analytical Chemistry* **2022**, *94* (33), 11610-11618.
- 37. Gaudreau, L.; Tielrooij, K. J.; Prawiroatmodjo, G. E. D. K.; Osmond, J.; de Abajo, F. J. G.; Koppens, F. H. L., Universal Distance-Scaling of Nonradiative Energy Transfer to Graphene. *Nano Letters* **2013**, *13* (5), 2030-2035.
- 38. Hu, Q.; Jin, D.; Xiao, J.; Nam, S. H.; Liu, X.; Liu, Y.; Zhang, X.; Fang, N. X., Ultrafast fluorescent decay induced by metal-mediated dipole–dipole interaction in two-dimensional molecular aggregates. **2017**, *114* (38), 10017-10022.
- 39. Singh, P.; Joshi, J., Nonradiative energy transfer and ion-ion interactions in terbium-praseodymium coactivated borate glass. *Journal of Luminescence* **2018**, *203*, 331-335.
- 40. Singh, M. R.; Guo, J.; Fanizza, E.; Dubey, M., Anomalous Photoluminescence Quenching in Metallic Nanohybrids. *The Journal of Physical Chemistry C* **2019**, *123* (15), 10013-10020.
- 41. Xu, J. X.; Liu, M.; Athukorale, S.; Zou, S.; Zhang, D., Linear Extrapolation of the Analyte-Specific Light Scattering and Fluorescence Depolarization in Turbid Samples. *ACS Omega* **2019**, *4* (3), 4739-4747.

TOC Figure:

